ADVANCED MATERIALS
www.advmat.de

www.MaterialsViews.com

Active Matrix-Based Collection of Airborne Analytes: An Analyte Recording Chip Providing Exposure History and Finger Print

*Jun Fang, Se-Chul Park, Leslie Schlag, Thomas Stauden, Jörg Pezoldt, and Heiko O. Jacobs**

The desire to detect and identify trace amounts of airborne analytes, including combustible or toxic gases, small molecules, particles, viruses or bacteria with ever increasing sensitivity and selectivity continues to be one of the main drivers in sensor research and analytical science.[1–3] A common approach in recent years has been to integrate the required analytical components into a small form factor to allow "onsite" detection at low cost. However, there are many cases where complexity and physical laws prevent scaling to small dimensions. For example, recognition by morphology still requires analyte specific forms of microscopy.[4,5] Equally, recognition by electromagnetic properties requires appropriate spectroscopic methods.[6,7] Independent of the specific situation, these techniques are relatively complex and are often performed at centralized "offsite" facilities. In all cases, it is usually required that the analyte is collected on the surface of a sensor (for onsite detection) or substrate (for offsite detection), which brings up the question of how to transport an airborne analyte to the target surface. The collection is often based on diffusion-only-transport whereby the analyte reaches the substrate on a random walk at a low rate.[8–12]

Different from this practice, this communication discusses ideas and first experimental results towards an active matrix based analyte collection approach referred to as "Airborne Analyte Memory Chip/Recorder", which (i) takes samples of the particles or molecules in an aerosol at specific points in time, (ii) transports the analyte sample to a designated spot on a surface, (iii) concentrates the analyte at this spot to achieve an amplification, (iv) repeats this sequence until the recording matrix is full, and (v) reads out the analyte matrix on the chip. The approach discussed here uses a directed force to transport and concentrate analytes at predetermined points on a surface at a rate which exceeds non-directed diffusion-only-transport by several orders of magnitude. The approach has recently become relevant considering a trend in sensor designs, which has focused on the reduction of the active sensor size to increase the sensitivity to a point where it is possible to detect single binding events.[13–16] At present most reports used diffusion-only-transport as a method, by which the analyte is transported to the sensing elements. Considering the fact that the sensing element is shrunk down to point like structures, diffusion-only-transport is not the best approach. Specifically, basic gas laws show that the number of analyte particles impinging on a surface goes to zero for point like structures. In other words, it becomes increasingly unlikely for an analyte molecule at low concentrations to "find" and interact with an ever increasingly small sensor, trading the gained sensitivity with a slow response time. The solution to this problem is to use a directed force to transport the analyte from a distance away to predetermined sensing points at a higher rate, which has recently been discussed elsewhere.[17–19] This communication adds the ability to collect and store analytes in an active matrix array like fashion, at predetermined points on a surface, at different points in times. As a consequence, the technique is able to provides a time record or memory of the events that occurred in the past yielding an average exposure, peak exposure, and exposure of various species on an as needed basis.

The approach is inspired by developed transport strategies in the aerosol community to collect airborne particles using convection,[20] thermophoretic,[21] magnetic,[22] and Coulomb[23,24] forces. The use of Coulomb forces has been chosen since localized collection of organic[25] and inorganic nanoparticles[26–29] has already been demonstrate with an unmatched sub 100 nm lateral resolution. While some sensors based on electrostatic precipitators are known,[17–19,30] an active matrix type analyte collection chip has not yet been demonstrated. This communication reports the collection of analytes over a wide range of molecular weights including (i) microscopic particles (Kentucky blue grass pollen, 20 µm in diameter, ~3×10^{17} Da), (ii) inorganic nanoparticles (Cu nanoparticles, 40–60 nm in diameter, ~3.5×10^{8} Da; CdSeS/ZnS nanoparticles, 6 nm in diameter, ~3.4×10^{5} Da), all the way down to (iii) small organic molecules (MEH-PPV, 1.5×10^{5}–2.5×10^{5} Da; Alq_3, 459.43 Da; anthracene, 178.23 Da; 4-fluorobenzenethiol 128.17 Da; benzenethiol, 110.19 Da). In the currently analyzed cases we find that the collection amount is increased by several orders of magnitudes comparing to the case where collection is driven by diffusion-only-transport. In addition to conventional microscopic analytical techniques, and to provide a quantitative analysis, we demonstrate that the collection scheme is compatible with more sophisticated analytical concepts, and specifically

J. Fang, S.-C. Park
Electrical and Computer Engineering
University of Minnesota
200 Union St. SE
Minneapolis, MN 55455, United States
L. Schlag, Dr. T. Stauden, Dr. J. Pezoldt,
Prof. Dr. H. O. Jacobs
Fachgebiet Nanotechnologie
Ilmenau University of Technology
Gustav-Kirchhoff-Strasse 1
D-98693, Ilmenau, Germany
E-mail: heiko.jacobs@tu-ilmenau.de

DOI: 10.1002/adma.201402589

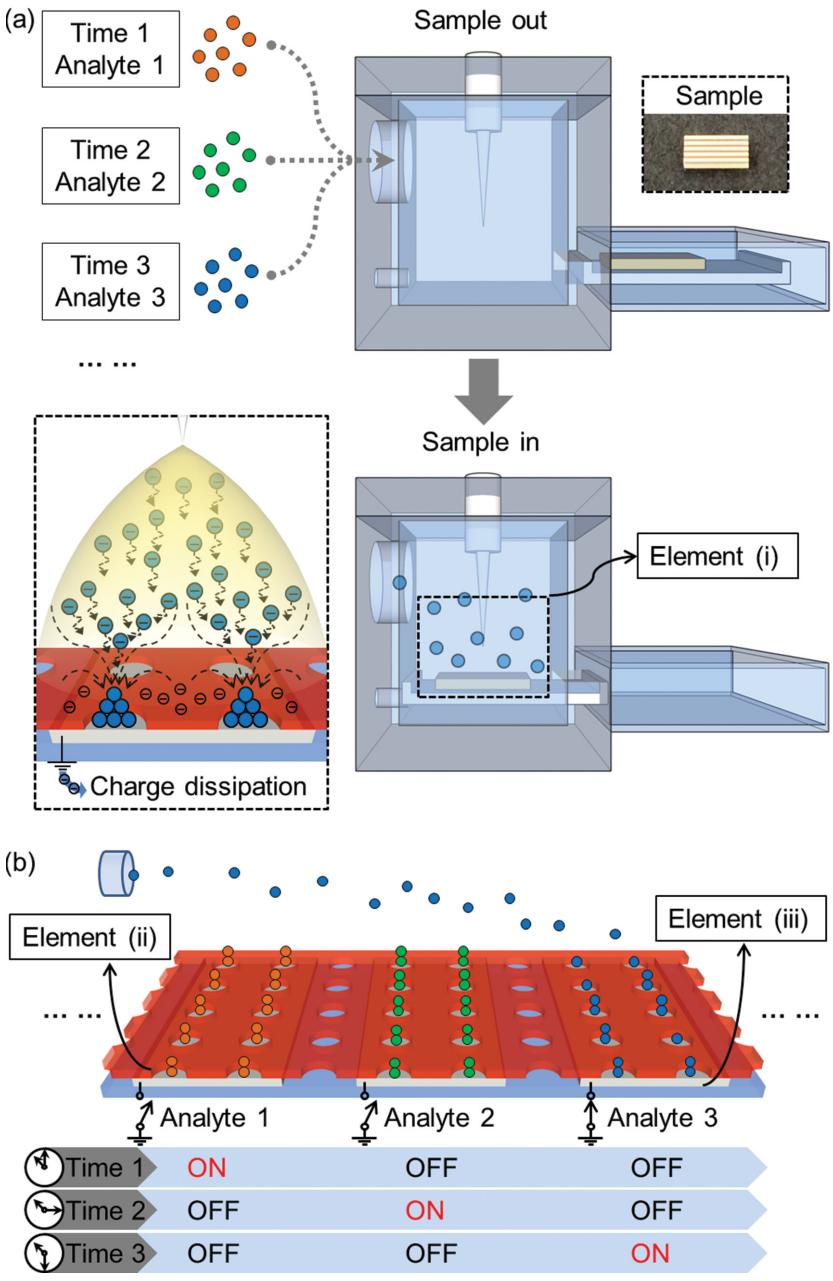

Figure 1. Schematic of the experimental recording platform to collect analytes in aerosols at known concentrations and different times using an "Analyte Memory Chip/Recorder" incorporating three design elements: (i) a Corona discharge based analyte charging method, (ii) an electrodynamic lens based analyte concentration concept (red insulating negatively charged film with openings), and (iii) an electrically biased domain electrode based active matrix design (grey electrodes underneath the red film).

with surface-enhanced Raman spectroscopy (SERS) to provide a signature and finger print of adsorbed molecular layers.

Figure 1 describes the experimental testing platform and the realized "Analyte Memory Chip/Recorder" that is used to test aerosols containing a variety of analytes at a known concentration. The "Analyte Memory Chip/Recorder" incorporates three design elements: (i) a Corona discharge based analyte charging method, (ii) an electrodynamic lens based analyte concentration concept, and (iii) an electrically biased domain electrodes based active matrix design to enable analyte collection and storage in selected recording sites at selected times. All analyte collection experiments use the collection chamber depicted in Figure 1(a) which was machined out of an insulating acrylic block to provide a 3 cm × 3 cm × 3 cm cavity, a 10 mm in diameter gas inlet, a 3 mm gas outlet, a pointed copper electrode 5 mm above the sample, a sample port and a sample tray. At 5 mm distance between the electrode and the sample, a Corona discharge can be generated using a 12 V–5 kV solid state high voltage converter (Gamma High Voltage Research, Inc., MC50). At a much shorter distance, a high current breakdown occurs which damages the substrate. Equally, at a much larger distance, we were not always able to get a stable Corona discharge using this converter. The sample tray was designed so that it can be shifted back and forth between two sealed positions. This design maintains the constant concentration of analytes in the chamber and enables a short exposure time. Analytes from various origins (discussed later) are introduced to the collecting chamber at different times. The Corona discharge occurs only as the sample (with a grounded domain electrode) is shifted to the exposure position which is underneath the negatively biased pointed electrode. Details of the Corona discharge based analyte charging method have been published previously.[19] In short, positive ionization occurs within a fairly thin ionizing plasma region (not shown),[31] where the electric field is sufficiently strong to cause the emission of electrons through the photoelectric effect which subsequently produce positive gaseous species and secondary electrons through impact ionization.[32] Beyond this region (shown), electrons with energy lower than ionization energy will attach to neutral analytes yielding negatively charged analyte particles. These negatively charged species move downwards until they reach the grounded collection electrode. When compared to conventional point to conducting plate Corona discharge experiments,[33] this report adds a patterned dielectric thin film with openings to the conductive plate to form a single or arrays of lensing structures. The purpose of the introduced dielectric lensing structures is to provide an electrodynamic funnel to transport the analyte from a distance away to desired collection points. The function of this design element has been reported previously.[26] In brief, the dielectric lensing structure is negatively charged through the deposition of electrons, which in turn produces the depicted fringing field. In our case, this design element is used to divert

the charged analytes to the desired points and to increase the flux and concentration of adsorbed materials in small points leading to an amplification of the analyte. Figure 1(b) incorporates all three design elements, adding "the externally biased domain electrodes" to the conceptual approach to achieve an active matrix like collection system. The domain electrodes that are left floating represent the OFF position (charge dissipation disabled); charge dissipation and steady state collection of analyte is blocked on floating electrodes. On the other hand, the domain electrode connected to ground represents the ON position (charge dissipation enabled). Collection of the analytes occurs on these domain electrodes at a level that is several orders of magnitude higher (discussed later) than in regions that are not electrically connected. The advantage of keeping regions floating and others connected to ground is that it leads to a self-equilibrating potential profile, whereby the transporting field of the charged analyte points to the grounded collection sites. Locally the field cannot point towards floating regions. If it would, the potential profile would adjust since no charge dissipation is possible on floating domains on a steady state basis.

Figure 2 provides results of a first set of experiments testing the "Corona/lens-based-collection" (design elements 1 and 2) concept to demonstrate that the process is generally applicable independent of the analyte type. The use of more than one domain electrode (active matrix, design element 3) will be discussed later. In the particular set of experiments a periodic electrodynamic lens array is used. The lens array is defined using a patterned 500 nm thick layer of insulating photoresist (s1805, Microposit) with 200 µm square (Figure 2(a)) or 1 µm circular (Figure 2(b-h)) openings to a flat silicon substrate which forms a single equipotential domain. All chips were 5 mm wide and 10 mm long.

In the experiments we tested a wide spectrum of aerosols. **Table 1** provides a list of the analytes, their concentrations, weights, and sizes. The goal was to test and demonstrate collection of analytes over the largest possible range of molecular weights to illustrate the generality of the approach. As a consequence several different aerosol preparation methods had to be used. The preparation details are included in the Supporting Information (Figure S1). In short (i) atomization of a liquid containing suspended solid or dissolved analytes was used in the case of Cu nanoparticles, CdSeS/ZnS nanoparticles, MEH-PPV, and Alq_3; (ii) direct thermal evaporation of a solid analyte was used in the case of anthracene; and (iii) evaporation of a liquid analyte inside a bubbler was used in the case of 4-fluorobenzenethiol (4-FBT) and benzenethiol (BT). All analytes were introduced to the testing chamber using 2000 sccm of N_2 as a carrier gas. A negative Corona discharge (–5 kV) was applied between the tip and the chips during a 1 second exposure time. The optical/fluorescent micrographs and SEMs illustrate the range of analyte particles that can be collected depicting Kentucky blue grass pollen (Figure 2(a)), Cu (Figure 2(b)) and CdSeS/ZnS (Figure 2(c)) nanoparticles, all the way down to small molecules such as MEH-PPV (Figure 2(d)), Alq_3 (Figure 2(e)), anthracene (Figure 2(f)), 4-FBT (Figure 2(g)) and BT (Figure 2(h)).

From an experimental point of view the following general results and observation are important: First, independent of

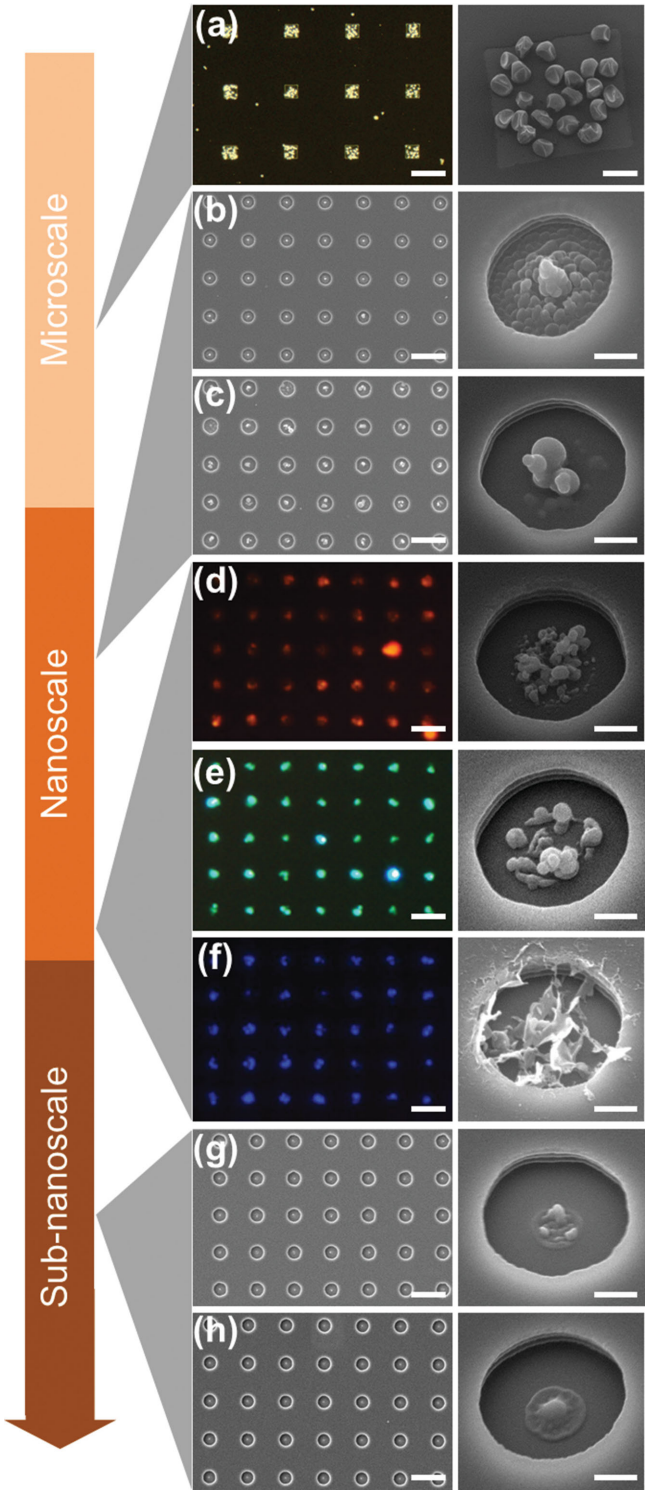

Figure 2. Micrographs of Corona/lens-based-collection of various analytes representing a wide range of molecular weights (from 3×10^{17} to 1×10^{2} Da). (a) Optical microscope image of locally collected Kentucky blue grass pollen. (b-c) SEM images of locally collected Cu nanoparticles and CdSeS/ZnS nanoparticles. (d-f) Fluorescent microscope images of locally collected MEH-PPV, Alq_3 and anthracene. (g-h) SEM images of locally collected 4-fluorobenzenethiol and benzenethiol. SEM closeups for each analyte are shown on the right. The scale bars are 500 µm in (a, left), 50 µm in (a, right), 5 µm in (b-h, left) and 500 nm in (b-h, right).

Table 1. List of the analytes, their concentrations, weights, and sizes.

Analyte	Concentration	Weight	Size
Pollen	Unknown	~3×10^{17} Da	~20 μm
Cu nanoparticles	<1 ppb	~3.5×10^{8} Da	~40–60 nm
CdSeS/ZnS nanoparticles	~99 ppb	~3.4×10^{5} Da	~6 nm
MEH-PPV	~168 ppb	1.5×10^{5}–2.5×10^{5} Da	~5 nm
Alq_3	~73 ppm	459.43 Da	~2 nm
Anthracene	~750 ppm	178.23 Da	~1 nm
4-FBT	~19 ppm	128.17 Da	~3 Å
BT	~9 ppm	110.19 Da	~3 Å

analyte type or size, it is possible to transport, concentrate, and collect the various analytes at predetermined sensing points using the introduced Corona/lens-based-collection process, which is remarkable considering the large range of analytes we tested. In terms of molecular weight the results represent a range of 3×10^{17} to 1×10^{2} Da. Second, the structures and at least some of the relevant physical properties remain intact. For example: (i) shape of the pollen particles; (ii) element composition of Cu and CdSeS/ZnS nanoparticles (EDS characterization data is available in Supporting Information, Figure S2); (iii) fluorescent characteristics of the MEH-PPV, Alq_3 and anthracene molecules; and (iv) spectral response due to Raman scattering (discussed later) of BT and 4-FBT, remain intact. Third, the localized collection rate is large comparing to commonly used approach where the analytes deposit randomly on the surface by diffusion-only-transport. In the case of BT and 4-FBT (quantitative measures will be provided later), the collection rate was determined to be 3 orders of magnitude faster than diffusion-only-transport. This is remarkable since it means that it should be possible to achieve an electrically driven collection/storage approach of analytes in addressable points without having a high level of cross contamination due to the diffusion-only-transport. The gained knowledge leads to the following active matrix idea using biased domain electrodes.

Figure 3 provides a set of results which combines and compares all design elements of the active matrix based analyte collection/storage chip. This set of experiments uses the introduced domain electrodes to control the material flux spatially in an active matrix array like fashion. The images in Figure 3(a) use domain electrodes without dielectric lensing structures while the images in Figure 3(b) represent the results where a dielectric lensing structure is added to increase the analyte concentration locally. The conceptual drawing is shown next to the results. In all cases, domain electrodes (gray region) that are left floating represent the OFF position (charge dissipation disabled). On the other hand, the domain electrode connected to ground represents the ON position (charge dissipation enabled). Experimentally the concept is tested using an insulating sapphire chip that provides a support to electrically isolated electrodes fabricated by standard photolithography. The size of the chips was 5 mm × 10 mm carrying 0.5 mm wide Ag strips with a 0.5 mm gap. Each chip had 5 electrically separated collecting domains. Again the illustrated 1 μm in diameter dielectric lensing structures (red layer) act as funnels for the analyte to be concentrated in predetermined points. The layer is identical to the one used in the description in Figure 2.

Samples of the aerosols in the test chamber were taken at different times. The test chamber contained Alq_3 at time 1 (10:00 AM), MEH-PPV at time 2 (10:15AM), BT at time

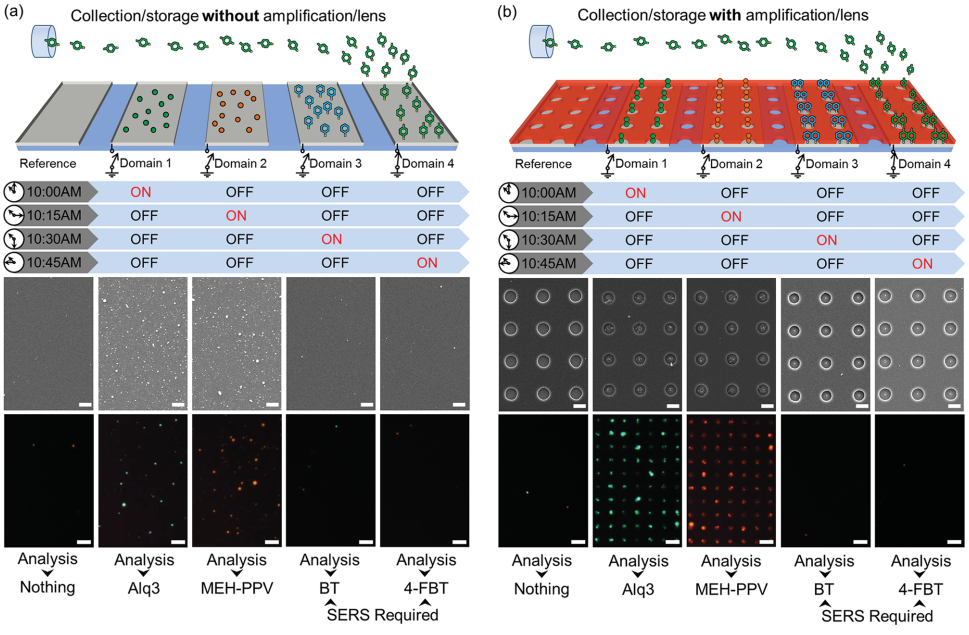

Figure 3. Active matrix based analyte collection/storage using externally biased domain electrodes (a) without and (b) with localized lens based concentration/amplification. Each domain represents a memory cell which collects analyte at a specific point in time through the application of electrical ground leading to a time record of past events. SEM and fluorescent microscope images of locally collected Alq_3, MEH-PPV, BT and 4-FBT are shown as first set of analytical tools to read out past events. The introduced lens leads to an amplification/increase of the analyte concentration in predetermined spots which aids in the detection. The scale bars are 1 μm for SEM images and 5 μm for microscope images.

3 (10:30AM), and 4-FBT at time 4 (10:45AM). The sampling time was 1 second in all cases under a –5 kV negative Corona discharge. Generally we find that there is little crosstalk between the individual domains which means that diffusion-only-transport is much slower that the Corona based analyte transport onto the biased domains. For example, the electrically floating reference domain (far left) does not show detectable amounts of precipitates on the surface which means that diffusion-only-transport is much slower than directed Corona-based-transport.

Out of the four analytes, two had a fluorescent signature Alq_3 (domain 1, green) and MEH-PPV (domain 2, red) and the location of the fluorescence confirms the storage of the analyte at the correct site. Domain 3 and 4 were used to collect BT and 4-FBT molecules which are very small molecules without any fluorescent properties. As anticipated no detectable amount of fluorescence is visible in these domains, which means that cross contamination through diffusion-only-transport from the surrounding domains can be neglected. Comparing the images in Figure 3(a) with the images in Figure 3(b) provides a qualitative measure of the analyte amplification factor that can be gained introducing the lensing structures. Each lens funnels the flux of analyte to a specific collection point, forming an array of analyte hotspots that help detection. The SEM images in domain 3 and 4 show small amounts of precipitates inside of the center of each lens. Again the Alq_3 and MEH-PPV were fairly straight forward substances that simplified the detection based on fluorescence microscopy. This is not the case considering the BT (domain 3) and 4-FBT (domain 4) containing aerosol. Although the analytical techniques used in Figure 3 (b, SEM, lens opening center) suggest that some precipitates are present, an identification is not possible using the presented data. The following section will carry out an experiment which will confirm that the visible precipitates contain the target molecules. The experiment uses surface enhanced Raman spectroscopy (SERS) as an analytical tool.

This section demonstrates and quantifies how this general strategy improves the collection efficiency of an existing SERS sensor design. Specifically, we integrated the collection scheme on an existing SERS sensor that is sensitive to the adsorption of small molecules such as BT and 4-FBT discussed previously. **Figure 4** provides a schematic of the designs we tested. Instead of using a simple Ag strip, the particular SERS sensor requires the use of an AgFON enhancing layer, which stands for a "standard" in the field of SERS detection.[34] In brief, the AgFON enhancing layer is a closely packed self-assembled layer of 150 nm in diameter silica nanospheres, where the top half is coated with 20 nm/180 nm Cr/Ag (Supporting Information, Figure S3). In addition, we introduce lensing structures (design element 2) and biased domains (design element 3) in the schematic (Figure 4, top). The white regions are conducting Ag coated silica nanospheres which are surrounded by uncoated insulating regions. The white conductive regions represent

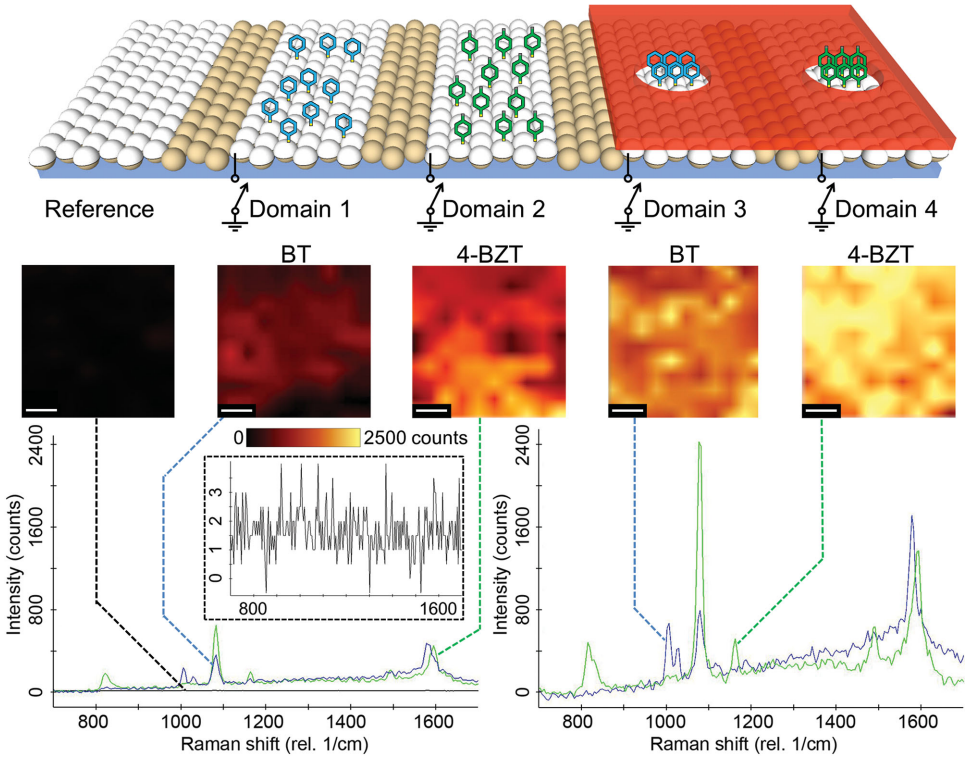

Figure 4. Recording elements integrated on a SERS sensor, illustrating schematics (top), next to corresponding Raman microscopy intensity maps at 1075 cm^{-1} (middle), and resulting spectra (bottom). BT analyte is collected on domain 1 and 3, and 4-FBT is collected on domain 2 and 4, respectively. On domain 3 and 4, a 0.5 mm thick PDMS mask with a 0.2 mm opening is used as an electrodynamic lens to achieve an amplified analyte collection. Raman intensity maps show raw unprocessed data recorded at 1075 cm^{-1} using the same microscope settings. Raman spectra represent an average recorded by the instrument over a 5 μm × 5 μm sized region. An offset (up down) correction has been applied for the spectra to overlap at the beginning of the graph. Peak height measurement and relative comparison is not effected. The scale bars are 1 μm.

the domain electrodes to control the collection/storage of analytes using the Corona-based-transport. On domain 3 and 4, a 0.5 mm thick PDMS film (shown in red) with an opening of 0.2 mm is used as the lens forming element. The reason to use PDMS is that it creates a good contact upon placing it onto the SERS layer, it can be removed during optical characterization, it can be reused, and most importantly it will not alter the sensing area. The same aerosol containing analytes as previously described were used. Specifically, BT (9 ppm) and 4-FBT (19 ppm) molecules are charged using a negative Corona discharge (–5 kV).

During the collection process, domain 1, 2, 3 and 4 are turned on (grounded) sequentially to store whatever analyte is present in the aerosol at the respective time at predetermined storage sites. Only one electrode is grounded each time for about 1 second and the others are left floating. The placement of the substrate is slightly shifted each time so that the tip is vertically above the grounded domain. We always took the region that is in the center of the strips for a relative comparison since there is a drop in the concentration within the edge region of the strips. The tapered region is fairly narrow typically less than 1 mm wide (Supporting Information, Figure S4). The molecules were recorded using Raman microscopy three days later which means that the information can be retained for a sufficiently long time. All Raman microscopy intensity maps (Figure 4, middle) and resulting spectra (Figure 4, bottom) were recorded under identical exposure and recording conditions to provide a relative comparison of the various design elements. The results are interesting: First, the reference domain shows again no detectable signal and a much longer (0.5 to 1 hour) exposure time is required to detect signatures of the target molecules on floating "diffusion-only-transport-domains" (Supporting Information, Figure S5). This agrees with previous result and means that diffusion-only-transport is not fast enough to cause a detectable signal in 1 second. Second, on domain 1 and 2, a dramatic increase in the signal (350 and 639 counts at 1075 cm^{-1}, respectively) is observed. This again agrees with previous results and means that introduced Corona based transport in combination with biased domains is highly efficient in the collection of all kinds of particles all the way down to molecular sized species. The location of the peeks of Raman spectra remain consistent with published values for BT and 4-FBT,[17] indicating the relevant physical properties remain intact. Third, the introduction of the electrodynamic lens based design elements on domain 3 and 4 leads to an additional amplification (increased to 831 and 2456 counts at 1075 cm^{-1}, respectively) due a localized increase in the amount of analyte that is collected. This is interesting since the diameter of lens opening is a factor of 200 times larger than what was used in Figure 3 which means that the lensing effect is not limited to a predetermined opening of only one diameter.

To provide a relative comparison of the effectiveness of the various design elements we made an attempt to provide a first order estimate by comparing the signal intensity recorded at 1075 cm^{-1} on the 5 different domains. Since the diffusion-only-transport-domain (reference domain) is not showing a detectable amount of material, a relative comparison would lead to large errors. To prevent this we ran additional experiments with a 10 second long exposure and were able to record 8 counts for BT and 15 counts for 4-FBT (Supporting Information, Figure S6) at 1075 cm^{-1} on electrically floating diffusion-only-transport-domains. The extrapolation provides a base level of 0.8 counts for BT and 1.5 counts for 4-FBT considering a 1 second long exposure. In terms of a relative comparison, the design elements "(i) Corona discharge based analyte charging method" in combination with the "(iii) electrically biased domain electrodes" increases the collection of the analytes by at least a factor of 400 (specifically, 437 and 426 in domain 1 and 2, respectively) when compared to the standard diffusion-only-transport approach. This number can further be increased to a factor exceeding 1000 (specifically, 1038 and 1637 in domain 3 and 4) through the introduction of the design element "(ii) electrodynamic lens", which provide a localized amplification of the analyte on the biased domain electrodes. In other words, the introduced collection and amplification process are highly effective to collect and locally store analyte at predetermined points. The recorded signals are 2 to 3 orders of magnitude higher when compared with the standard diffusion-only-transport approach. While this appears to be a very large number we think that this is a conservative estimate in terms of amount of material that is collected. Considering that the Raman signal saturates under excessive material coverage the intensity measurement would suggest that the actually collected material exceeds these estimates.[35] Moreover, it should be possible to increase the values further through optimization of the opening size, pitch, domain size and domain potential. For example a smaller pitch and higher potential should allow a further increase in the amount of material that can be collected locally compared with the standard diffusion-only-transport approach.

Figure 5 provides a result where the introduced analyte recording chip is used to retrieve past/historical analyte concentration. Samples of the environment were collected in 30 minutes intervals providing a time record over a 12 hour period. Specifically, the analyte (BT) concentration was randomly set to be 2 ppm, 4 ppm, 6 ppm, 8 ppm or 10 ppm during the collection cycle. The collection process is identical as previously described. After the collection, the offsite SERS data taken from the various domains again allow an identification of the BT. For each domain/time, the Raman signal intensity at 1075 cm^{-1} is recorded (line). We repeated the experiment over a period of three days using the same analyte sequence and the plot indicates the mean value and deviation (STD). The actual analyte concentration of the aerosol is shown as well to provide a comparison (bars). The comparison shows that it is possible to retrieve the information of prior exposure concentrations. We have not yet established the ultimate limits of how many recording sites can be integrated. The number 25 is currently only limited by the number of electrical connections that we can make and handle. The experiment in Figure 5 used five chips whereby each chip had five electrically separated domains.

In conclusion, the application of the discovered process as an active matrix analyte recording chip has been limited by the number of electrical connections that we can make. From a practical point of view, a multiplexing concept would have to be introduced to further increase the number of isolated recording sites. From a physical point of view, however, it should be possible to achieve a larger number of recording sites than what

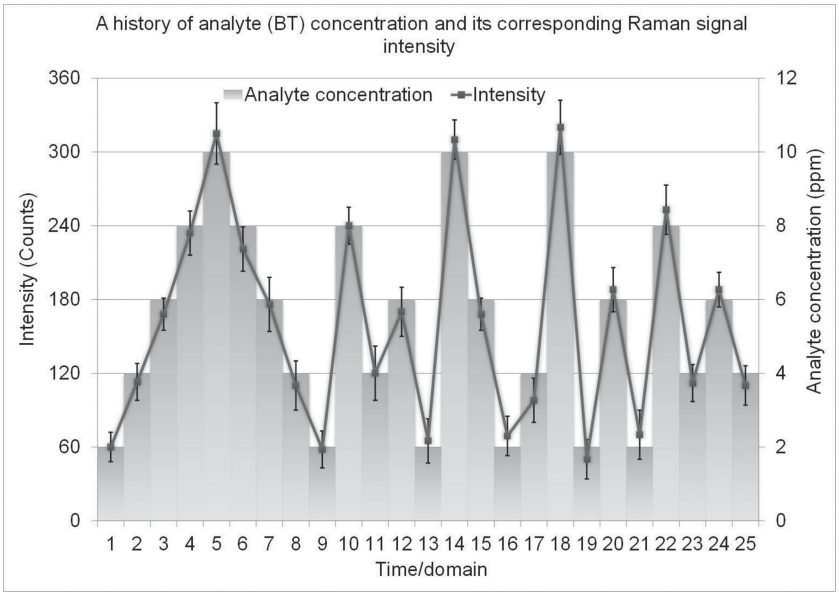

Figure 5. Recovered BT analyte concentration measured as Raman counts (line, Raman signal intensity at 1075 cm^{-1}) analyzing 25 recording sites. The actual analyte exposure concentration (bars, in ppm) is used as a background to help in the comparison. In the experiment, 25 sequentially grounded domain electrodes were used to record the concentration of BT over a period of 12 hours using a 1 second long sampling time every 30 minutes. The concentration of BT was randomly changed every 30 minutes to be 2 ppm, 4 ppm, 6 ppm, 8 ppm or 10 ppm. The recovered signal intensity (red line) agrees well with the actual concentration.

has been demonstrated. The spatial resolution (spot size was 1 μm in Figure 3 and 200 μm in Figure 4) suggest that a much higher integration density can be attained. However, crosstalk rather than integration density, is likely going to be the limiting factor. Specifically, the analyte transport based on random diffusion was 400 to 1000 times slower than the directed transport method used in this study. This means that it should be possible to record a sequence of 400 to 1000 analyte exposures before diffusion based cross-contamination becomes the limiting factor. The basic idea is that such a chip could be a commodity item that is placed in an environment that a user would like to keep a record from. The information is retrieved on an as needed basis. Offsite analysis of the chip storing the information would make this approach more economical than an online monitoring system for all kinds of threads. The conceptual approach of a simple recording device can be compared to RADON collectors that are placed into millions of households in the US for a period of time to record an integral value of RADON exposure. The recording container is closed and returned to centralized analytical facility, which measures the accumulated exposure dosage using expensive analytical tools to reduce the cost and maintain a standard. Our approach is different in the sense that it provides a time record.

A second and more immediate application relates to improvements in the response time that can be gained using the directed transport schemes that have been introduced. For example, a 1 second long exposure to BT analyte was sufficient to obtain 350 counts at the characteristic 1075 cm^{-1} peek (Figure 4, blue, without lens) which is a short time considering the low analyte concentration (9 ppm) that was used in the experiment. It is not possible to detect such a low analyte concentration using the diffusion-only-transport standard unless a much longer exposure time is used. For example, it took a 1 hour long exposure using diffusion-only-transport to achieve the same signal intensity level (Supporting Information, Figure S5). This is perhaps the most important result of this study since this general trend holds true over a very large range of analyte particles (14 orders of magnitude in terms of molecular weight, Figure 2). As a consequence the approach should benefit any sensing concept that involves a surface sensor and not just SERS. What it means is that others adapting this concept should anticipate several orders of magnitude increases in response time over sensing systems that use diffusion-only-transport to the surface sensor they use.

Finally, the ability to direct analytes to nanoscopic sensing points using the nanolens is also relevant in light of recent research on nanosensors, where a trend has been to shrink down the active sensor area to a point to detect single molecular binding events. While this trend increased the sensitivity, it came at the price of a slow response time since it is increasingly unlikely for a molecule to "find" the nanoscopic sensing elements/points using the diffusion-only-transport, as impingement and capture rates scales with the area of the sensing element. As a consequence the introduced nanolens based transport can be employed to increase the collection speed and localized concentration of the analyte on nanoscopic sensing elements to acceptable levels.

Experimental Section

Aerosol Preparation: Various types of aerosols were used in this study. Specifically, we tested gas mixtures (aerosols) containing large microscopic particles Kentucky blue grass pollen, Cu and CdSeS/ZnS nanoparticles, all the way down to small molecules such as fluorescent MEH-PPV, Alq_3 and anthracene, non-fluorescent 4-fluorobenzenethiol and benzenethiol. All of the materials were purchased from Sigma-Aldrich. Figure S1 shows the schematic of the aerosol preparation methods: (a) Pollen (a loose powder) was carried into the collection chamber using 2000 sccm N_2 flow. It is used to show collection ability of an allergenic substance. (b) Cu and CdSeS/ZnS nanoparticles/MEH-PPV/Alq_3 containing aerosol was generated using atomization. Specifically, the aerosol containing Cu or CdSeS/ZnS nanoparticles were prepared using toluene solution (5 mg/mL). The solution was then dropped on an atomizer (an ultrasonic vibrating mesh) at a constant rate. The atomization rate was approximately 0.01 $mL{\cdot}s^{-1}$. The aerosol was further diluted with 2000 sccm N_2 which also serves as a carrier gas to transport the analyte into the collection chamber. The calculated concentration (using 3.5×10^8 Da for Cu and 3.4×10^5 Da for CdSeS/ZnS) was <1 ppb for Cu and ~99 ppb for CdSeS/ZnS. Similarly, MEH-PPV and Alq_3 was first dissolved in tetrahydrofuran (THF) solution (5 mg/mL), separately. The atomization rate was approximately 0.01 $mL{\cdot}s^{-1}$ which was further diluted with 2000 sccm N_2. The calculated concentration (using 2.0×10^5 Da for MEH-PPV and 459.43 Da for Alq_3) was ~168 ppb for MEH-PPV and ~73 ppm for Alq_3. (c) Anthracene containing aerosol was generated by thermal evaporation. Anthracene is a white

solid powder with a melting point of 210–215 °C. In this experiment, anthracene was thermal evaporated at 250 °C. The evaporation rate was estimated to be 0.2 $mg \cdot s^{-1}$ by measuring the weight reduction. The carrier gas was 2000 sccm N_2. The calculated concentration (using 178.23 Da) was ~750 ppm. (d) 4-flourobenzenethiol and benzenethiol containing aerosol was generated using bubbler based evaporation. Specifically, the analyte was introduced using a conventional bubbler approach with a flow rate of 10 sccm N_2 in the bubbler line. The vapor pressure of 4-flourobenzenethiol is 2.85 mmHg and benzenethiol is 1.4 mmHg at room temperature which is equivalent of 3800 ppm of 4-FBT and 1800 ppm of BT molecules inside the bubbler and 19 ppm of 4-FBT and 9 ppm of BT after dilution with 2000 sccm N_2.

Fabrication of AgFON Substrate: Silicon wafers were first put in HF solution for 30 s to remove the native oxide. The wafers were rinsed in acetone, methanol, IPA, DI water, and further cleaned in piranha etch at 120 °C for 30 min, and then in 5:1:1 ratio of H_2O:NH_4OH:H_2O_2 for 30 min to make the surface hydrophilic. Surfactant-free, silica nanosphere suspensions (Bangs Laboratories, Inc.) was further diluted in ethanol (1:1 volume ratio), which served as a spreading agent. The suspension was dropped onto a water surface which yields a surface layer of silica beads. The Langmuir-Blodgett method was used to compact the beads and to transfer the beads to the target wafer. After drying the surface for 30 minutes, the AgFON standard substrate was completed through e-beam evaporation of 20 nm/180 nm Cr/Ag films to form the plasmonic cap layer.

SERS Characterization: SERS spectra and corresponding Raman microscopy intensity maps were acquired using a confocal Raman microscope system (Witec Alpha 300R) equipped with an objective lens (Nikon 100×, 0.90 NA in air). A fibre-optic interfaced 514 nm argon ion laser was used as a laser source, which was set to a constant power of ~2 mW for all SERS measurements in this report. The lateral imaging resolution of the confocal system considering the wavelength, and numerical aperture of the system is ~300 nm. The scattered light was analyzed using a 600 mm^{-1} spectrometer grating with a spectral resolution of about 3 cm^{-1}. The collection area was defined by a 5 μm × 5 μm region with a 10 × 10 sampling density. The collection time for each sampling spot was 1 second. The reflectance absorption spectrum was analyzed using a VIS-NIR spectrophotometer (Ocean Optics, USB4000 VIS-NIR spectrometer, QR400–7-UV–vis reflection probe). The reflectance absorption spectrum of AgFON was collected and used for the chosen wavelength (514.5 nm).

Supporting Information

Supporting Information is available from the Wiley Online Library or from the author.

Acknowledgements

The research received financial support in part through grants from the National Science Foundation (NSF Grant DMI-0755995), German Science Foundation (DFG Grants STA 556/4–1 and JA 1023/4–1), and the Carl-Zeiss Foundation.
Note: Figure 5 was replaced on December 1, 2014, after initial publication online.

Received: June 11, 2014
Revised: August 26, 2014
Published online: October 27, 2014

[1] F. Favier, E. C. Walter, M. P. Zach, T. Benter, R. M. Penner, *Science* **2001**, *293*, 2227.
[2] F. Shen, J. Wang, Z. Xu, Y. Wu, Q. Chen, X. Li, X. Jie, L. Li, M. Yao, X. Guo, T. Zhu, *Nano Lett.* **2012**, *12*, 3722.
[3] M. D. Ward, D. A. Buttry, *Science* **1990**, *249*, 1000.
[4] Y. Y. Vengerov, T. E. Semenov, *Electron Microsc. Res.* **1992**, *2*, 193.
[5] N. Jalili, K. Laxminarayana, *Mechatronics* **2004**, *8*, 907.
[6] C. J. Benmore, *ISRN mater. sci.* **2012**, *2012*, 852905.
[7] P. L. Stiles, J. A. Dieringer, N. C. Shah, R. P. Van Duyne, *Annu. Rev. Anal. Chem.* **2008**, *1*, 601.
[8] K. Ikebukuro, C. Kiyohara, K. Sode, *Biosens. Bioelectron.* **2005**, *20*, 2168.
[9] P. Krebs, A. Grisel, *Sens. Actuators, B* **1993**, *13*, 155.
[10] T. Wagner, S. Haffer, C. Weinberger, D. Klaus, M. Tiemann, *Chem. Soc. Rev.* **2013**, *42*, 4036.
[11] M. S. Arnold, P. Avouris, Z. W. Pan, Z. L. Wang, *J. Phys. Chem. B* **2003**, *107*, 659.
[12] B. Ilic, D. Czaplewski, H. G. Craighead, P. Neuzil, C. Campagnolo, C. Batt, *Appl. Phys. Lett.* **2000**, *77*, 450.
[13] K. Besteman, J.-O. Lee, F. G. M. Wiertz, H. A. Heering, C. Dekker, *Nano Lett.* **2003**, *3*, 727.
[14] M. Li, H. X. Tang, M. L. Roukes, *Nat. Nanotechnol.* **2007**, *2*, 114.
[15] E. Hao, G. C. Schatz, *J. Chem. Phys.* **2004**, *120*, 357.
[16] M. Tsutsui, M. Taniguchi, K. Yokota, T. Kawai, *Nat. Nanotechnol.* **2010**, *5*, 286.
[17] E.-C. Lin, J. Fang, S.-C. Park, F. W. Johnson, H. O. Jacobs, *Nat. Commun.* **2013**, *4*, 1636.
[18] E.-C. Lin, J. Fang, S.-C. Park, T. Stauden, J. Pezoldt, H. O. Jacobs, *Adv. Mater.* **2013**, *25*, 3554.
[19] J. Fang, S.-C. Park, L. Schlag, T. Stauden, J. Pezoldt, H. O. Jacobs, *Adv. Funct. Mater.* **2014**, *24*, 3706.
[20] C. Kanaoka, H. Emi, W. Tanthapanichakoon, *AIChE J.* **1983**, *29*, 895.
[21] J. P. Black, A. Elium, R. M. White, M. G. Apte, L. A. Gundel, R. Cambie, *Proc. IEEE Ultrasonics Symp.* **2007**, 476.
[22] B. B. Yellen, G. Friedman, *Adv. Mater.* **2004**, *16*, 111.
[23] C. R. Barry, J. Gu, H. O. Jacobs, *Nano Lett.* **2005**, *5*, 2078.
[24] P. Mesquida, A. Stemmer, *Adv. Mater.* **2001**, *13*, 1395.
[25] A. M. Welle, H. O. Jacobs, *Appl. Phys. Lett.* **2005**, *87*, 263119.
[26] C. R. Barry, H. O. Jacobs, *Nano Lett.* **2006**, *6*, 2790.
[27] J. J. Cole, E.-C. Lin, C. R. Barry, H. O. Jacobs, *Appl. Phys. Lett.* **2009**, *95*, 113101.
[28] E.-C. Lin, J. J. Cole, H. O. Jacobs, *Nano Lett.* **2010**, *10*, 4494.
[29] J. J. Cole, E.-C. Lin, C. R. Barry, H. O. Jacobs, *Small* **2010**, *6*, 1117.
[30] J. Jang, D. Akin, K. S. Lim, S. Broyles, M. R. Ladisch, R. Bashir, *Sens. Actuators, B* **2007**, *121*, 560.
[31] K. Yanallah, F. Pontiga, *Plasma Sources Sci. Technol.* **2012**, *21*, 045007.
[32] M. Abdel-Salam, M. Nakano, A. Mizuno, *J. Phys. D: Appl. Phys.* **2007**, *40*, 3363.
[33] J.-S. Chang, P. A. Lawless, T. Yamamoto, *IEEE Trans. Plasma Sci.* **1991**, *19*, 1152.
[34] L. A. Dick, A. D. McFarland, C. L. Haynes, R. P. V. Duyne, *J. Phys. Chem. B* **2002**, *106*, 853.
[35] L.-J. Wan, M. Terashima, H. Noda, M. Osawa, *J. Phys. Chem. B* **2000**, *104*, 3563.